Ceramics International xxx (xxxx) xxx–xxx

Contents lists available at ScienceDirect

Ceramics International

journal homepage: www.elsevier.com/locate/ceramint

Microwave dielectric properties of glass-free $CaMg_{0.9-x}Li_{0.2}Zn_xSi_2O_6$ ceramics for LTCC applications

Fangyi Huang[a], Hua Su[a,c], Yulan Jing[a], Yuanxun Li[a,c], Qihai Lu[b,**], Xiaoli Tang[a,*]

[a] State Key Laboratory of Electronic Thin Films and Integrated Devices, University of Electronic Science and Technology of China, Chengdu, 610054, China
[b] Key Laboratory of Sensor and Sensing Technology of Gansu Province & Institute of Sensor Technology, Gansu Academy of Sciences, Lanzhou, 730000, China
[c] Jiangxi Guo Chuang Industrial Park Development Co., Ltd, Ganzhou, China

ARTICLE INFO

Keywords:
LTCC
Microwave dielectric properties
Rietveld refinement
Raman spectroscopy

ABSTRACT

Herein, glass-free microwave dielectric ceramics $CaMg_{0.9-x}Li_{0.2}Zn_xSi_2O_6$ (x = 0–0.36) with excellent microwave dielectric properties were prepared via traditional solid-state reaction method. Phase composition and crystalline structure were identified using X-ray diffraction (XRD), which confirmed that the ceramics contained more than one phase. Rietveld refinement method was utilized to analyze XRD data and obtain structural information, such as lattice parameters. SEM photographs showed that Zn^{2+} substitution could effectively promote densification of the ceramics. Microwave dielectric properties were obviously influenced by the combination of multiple phases. Combined with Raman spectra, influences of Raman shift and FWHM of vibration peaks on microwave dielectric properties were determined. The $CaMg_{0.9-x}Li_{0.2}Zn_xSi_2O_6$ ceramic exhibited high performance at x = 0.28 with: $Q \times f$ = 68,190 GHz, ε_r = 7.51 and τ_f = −68 ppm/°C, when sintered at 900 °C. The studied ceramics are promising candidates for LTCC application.

1. Introduction

Microwave dielectric ceramics are widely used in microwave communication devices [1,2], especially in the era of 5G technology. Low temperature co-fired ceramics (LTCC) technology is commonly used in order for such devices to meet the requirements of miniaturization, integration and functionalization [3–5]. Microwave dielectric ceramics with low permittivity are key materials of LTCC substrates that can generate effective signal delay reduction in the millimeter wave band, and should have low sintering temperature (lower than 961 °C), high quality factor and near zero temperature coefficient of resonance frequency (τ_f) as well as excellent thermal stability [6–9]. Three methods that lower the sintering temperature include addition of sintering aids, adopting glass-ceramic method and utilization of ultra fine powders [10]. However, the addition of sintering aids may deteriorate ceramics' dielectric properties [11]; the utilization of ultrafine powders will increase production costs; glass-ceramic method need high equipment requirements [12] and may leave glass phase causing the loss of performance. Furthermore, certain sintering aids such as V_2O_5 are toxic, and are not compatible with environmentally friendly production. Therefore, it is of great significance to study glass-free LTCC microwave dielectric ceramics, in which ion substitution is one of such methods.

Since $CaMgSi_2O_6$ is a silicate ceramic, it has good microwave dielectric properties with [13]:ε_r = 7.46, $Q \times f$ = 59,638 GHz and τ_f = −46 ppm/°C (sintered at 1290 °C). Therefore, it has the potential to develop LTCC substrate materials with low dielectric and low loss. In our previous work, it was found that Li ion could lower the sintering temperature of $CaMgSi_2O_6$ ceramic in conjunction with a small amount of LBSCA glass. However, dielectric loss was not successfully decreased. Studies have shown that zinc ion substitution could further improve microwave dielectric properties of the magnesium silicates while reducing sintering temperature. $Mg_{1-x}Zn_xSiO_3$ ceramics could enhance performance from 103,453 GHz (x = 0) to maximum 138,481 GHz (x = 0.15) when sintered at 1360 °C for 9 h, which significantly decreased the sintering temperature [14]. Dhanesh et al. [15] investigated the effects of Zn^{2+} substitution content on $LiMgPO_4$ ceramics' microwave dielectric properties and found that $LiMg_{0.9}Zn_{0.1}PO_4$ ceramics sintered at 925 °C exhibited perfect microwave dielectric properties: $Q \times f$ = 99,700 GHz, ε = 6.7 and τ_f = −62 ppm/°C, while sintering temperature decreased and $Q \times f$ value increased. Comparable results could be observed in other researches [16–18]. Obviously, substitution of Mg^{2+} with Zn^{2+} reduced sintering temperature and improved ceramic performance at the same time.

Furthermore, Raman spectroscopy and XRD analysis are often used

* Corresponding author.
** Corresponding author.
E-mail addresses: luqhis20@163.com (Q. Lu), tangtang1227@uestc.edu.cn (X. Tang).

https://doi.org/10.1016/j.ceramint.2020.05.052
Received 7 April 2020; Received in revised form 4 May 2020; Accepted 4 May 2020

to examine the microstructure of microwave dielectric ceramics, allowing further exploration into lattice vibration, orderness, crystallinity and cation distortion of the materials. Herein, we investigated the crystal structure, phase composition, microtopography and microwave dielectric properties of Zn^{2+} substituted $CaMg_{0.9-x}Li_{0.2}Zn_xSi_2O_6$ (x = 0–0.36) ceramics. Rietveld refinement method and Raman spectroscopy were applied to further analyze the effects of Zn^{2+} on material's structure and properties.

2. Experimental procedures

The $CaMg_{0.9-x}Li_{0.2}Zn_xSi_2O_6$ (x = 0–0.36) ceramics were synthesized via conventional solid-state reaction method with analytically pure raw materials: $CaCO_3$ (99.5%, Aladdin, Shanghai, China), MgO (nanoscale, 99.9%, Aladdin, Shanghai, China), Li_2CO_3 (99%, KESHI KL, Chengdu, China), ZnO (99%, Aladdin, Shanghai, China), SiO_2 (99.9%, Aladdin, Shanghai, China). All raw materials were weighed according to the molar ratios, then placed into nylon tanks with distilled water, and ball milled for 12 h. The ground-dried powders were poured into alumina crucibles and placed into muffle furnace, which were calcined at 900 °C for 3 h. Calcined powders were ball milled again for 6 h and then mixed with moderate PVA (10 wt%) for granulation, followed by particles with fluidity being pressed into cylinders 12 mm in diameter and 6 mm in thickness. The cylinders were sintered at temperatures of 875 °C, 900 °C, 925 °C and 950 °C for 3 h, respectively.

In order to identify the phase composition and crystal structure of the $CaMg_{0.9-x}Li_{0.2}Zn_xSi_2O_6$ ceramics, X-ray diffraction (XRD: MinFlex 600; Rigaku, Japan) and Raman spectra were employed. Meanwhile, the diffraction pattern was refined and fitted in Fullprof software [19] to obtain more information regarding crystal structure. Microstructure of the samples was determined by SEM (JSM-6490LV; JEOL, Japan) analysis. Archimedes principle based method was used to measure ceramics' bulk density. Theoretical density of each phase was calculated from Eq. (1), and multi-phase system from Eq. (2) [19]. Relative density was easily obtained by Eq. (3) [19]. The microwave dielectric properties of the samples were measured by Network Analyzer (N5230; Agilent Technologies, USA) in TE011 mode and τ_f could be calculated by Eq. (4).

$$\rho_{theo} = \frac{n \cdot A}{V \cdot N} \tag{1}$$

$$\rho_{theo} = \frac{W_1 + W_2 + W_3}{W_1/\rho_1 + W_2/\rho_2 + W_3/\rho_3} \tag{2}$$

$$\rho_r = \frac{\rho_{bulk}}{\rho_{theo}} \tag{3}$$

$$\tau_f = \frac{f_{85} - f_{25}}{f_{25}(85\,^{\circ}\mathrm{C} - 25\,^{\circ}\mathrm{C})} 10^6 \tag{4}$$

where n, A, V, N are the number of formula unit in a primitive cell, the molecular mass of the composition, the unit cell volume and Avogadro constant; ρ_1, ρ_2, ρ_3, W_1, W_2 and W_3 represent the theoretical density and weight fraction of phase1, phase2 and phase3 separately; And f_{25} and f_{85} are the resonant frequencies at 25 °C and 85 °C respectively.

3. Results and discussion

The XRD patterns of the $CaMg_{0.9-x}Li_{0.2}Zn_xSi_2O_6$ ceramics sintered at 900 °C for 3 h are displayed in Fig. 1 (a), where $CaMgSi_2O_6$ (PDF#72-1497) is the main phase, and the composition of secondary phase changes with increasing Zn^{2+} content. When x = 0, three phases of $CaMgSi_2O_6$, $CaSiO_3$ (PDF#84-0654) and Li_2SiO_3 (PDF#30-0766) are observed, as Li_2SiO_3 decreases a small amount of Li_2ZnSiO_4 (PDF#15-0056) is formed at x = 0.08, and afterwards Li_2SiO_3 completely transforms into Li_2ZnSiO_4 with further increasing x value. As Zn^{2+}

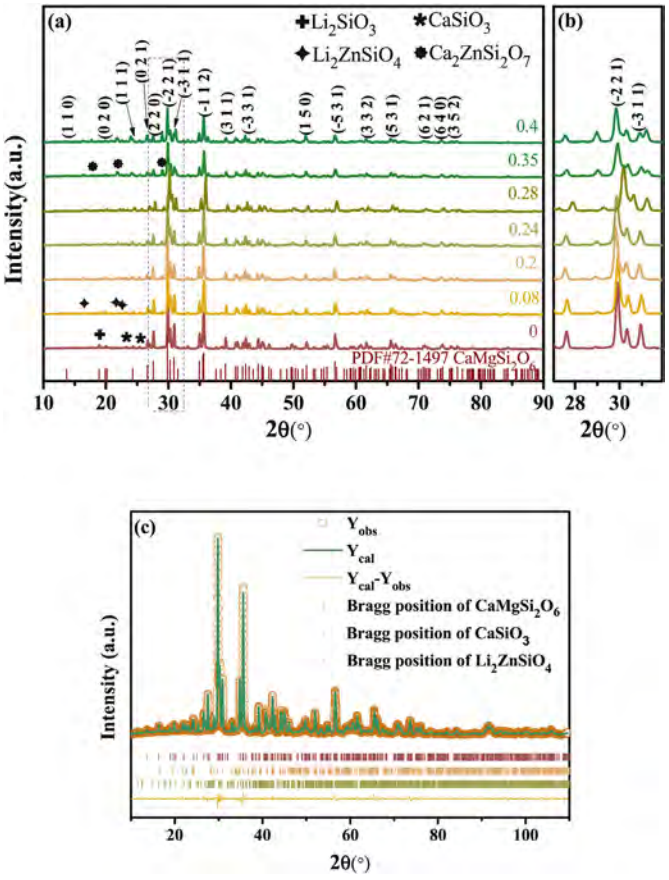

Fig. 1. (a) XRD patterns of the $CaMg_{0.9-x}Li_{0.2}Zn_xSi_2O_6$ (x = 0, 0.08, 0.2, 0.24, 0.28, 0.32, 0.36) ceramics sintered at 900 °C; (b) The amplification of the XRD patterns; (c) Refined plot of the sample with x = 0.28.

content increases to 0.32, a new $Ca_2ZnSi_2O_7$ (PDF#35-0745) phase is formed with decreasing Li_2ZnSiO_4 phase content, which makes four phases in the ceramics thus far. The appearance of the other phases might be the results of the same temperature of calcinating and sintering as well as the formation of finite solid solution by Zn^{2+} substitution [17,18,20]. Specific changes in phase composition and content could obtain from the subsequent XRD refinement data. Fig. 1 (b) shows the magnification of the characteristic peaks including (−221) and (−311) of main phase $CaMgSi_2O_6$. The characteristic peaks shift with increasing Zn^{2+} content due to changes in the crystal structure and lattice parameters.

XRD patterns of the samples sintered at 900 °C for 3 h were refined using Fullprof software. Monoclinic $CaMgSi_2O_6$ (*C12/c1*, a = 9.7397 Å, b = 8.9174 Å and c = 5.2503 Å, $\alpha = \gamma = 90^{\circ}$, β = 105.86°), triclinic $CaSiO_3$ (*P-1*, a = 7.9400 Å, b = 7.3200 Å and c = 7.0700 Å, α = 90.03°, β = 95.37°, γ = 103.43°), orthorhombic Li_2SiO_3 (*Cmc21*, a = 9.3600 Å, b = 5.3950 Å and c = 4.6750 Å, $\alpha = \beta = \gamma = 90^{\circ}$), monoclinic Li_2ZnSiO_4 (*P21/n*, a = 6.2620 Å, b = 10.6020 Å and c = 5.0210 Å, $\alpha = \gamma = 90^{\circ}$, β = 90.51°) and tetragonal $Ca_2ZnSi_2O_7$ (*P-421 m*, $a = b$ = 7.8279 Å and c = 5.0138 Å, $\alpha = \beta = \gamma = 90^{\circ}$) were adopted as models for refinement. The refined results including the reliability factors and more accurate information about the lattice of each phase are shown in Table 1 and Fig. 2. Fig. 1 (c) presents the refined fitting curves of $CaMg_{0.62}Li_{0.2}Zn_{0.28}Si_2O_6$ composite, where the high consistency between the fitted and measured curves is observed. The reliability factors in Table .1, especially χ^2 is adequately small, which proves the reasonableness and acceptance of the information presented in Fig. 2. Therefore, structural data obtained from the refinement can be used to explain the correlations between the structure and the dielectric properties. The trend of lattice constant b is in

Table 1
The profile factor (R_p), weighted profile factor (R_{wp}), expected weighted profile factor (R_{exp}) and reduced chi-square (χ^2) of the $CaMg_{0.9-x}Li_{0.2}Zn_xSi_2O_6$ (x = 0, 0.08, 0.2, 0.24, 0.28, 0.32, 0.36) ceramics from Rietveld refinement method.

x (mol)	0	0.08	0.2	0.24	0.28	0.32	0.36
R_p (%)	9.02	8.86	8.81	9.41	9.07	11.7	9.76
R_{wp} (%)	9.87	9.84	9.76	10.5	10.3	12.4	11.6
R_{exp} (%)	8.63	9.01	9.4	9.34	9.16	10.8	9.96
χ^2	1.31	1.19	1.08	1.27	1.28	1.32	1.35

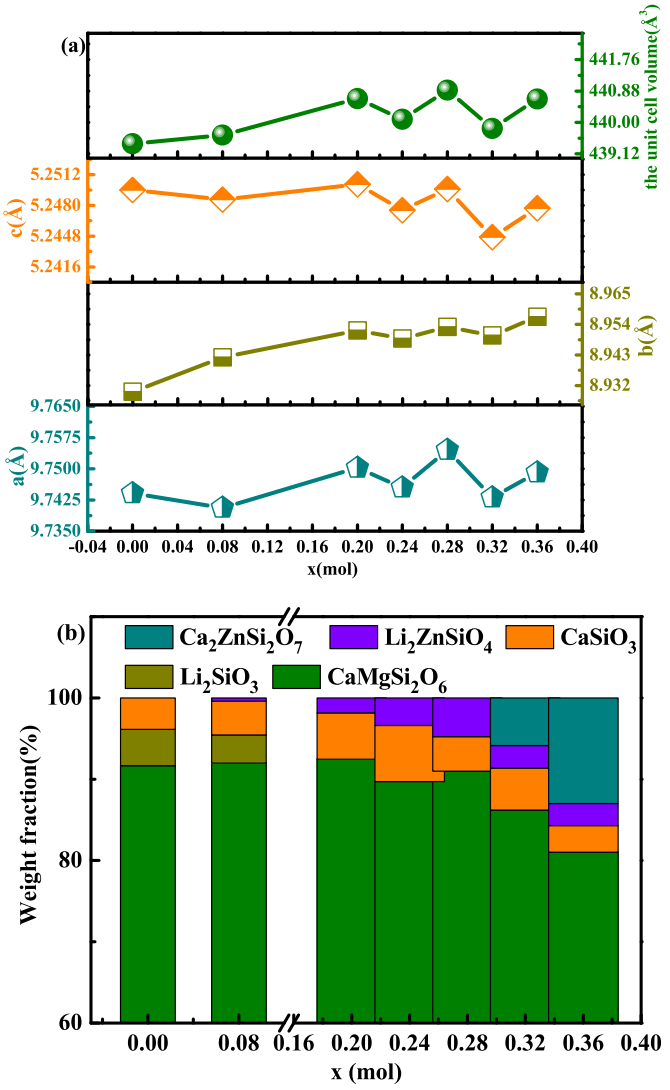

Fig. 2. (a) Lattice parameters, unit cell volume of $CaMgSi_2O_6$ phase (b) and the weight fraction of different phases.

accordance with that of unit cell volume for $CaMgSi_2O_6$ phase in Fig. 2 (a), which further promotes the shift of the diffraction peak to a smaller diffraction angle as the corresponding unit cell volume increases [21]. However, the relationship between peak-shifting and unit cell volume is abnormal around x = 0.28. The reason for the observed large right movement might be due to instrumental error. Fig. 2 (b) displays the weight fraction changing of composites. The major phase content varies nonlinearly with x value. Thus, Zn^{2+} greatly affected the phase composition and structure of ceramics, which in turn influenced the microwave dielectric properties.

Fig. 3 exhibits Raman spectra of the $CaMg_{0.9-x}Li_{0.2}ZnxSi_2O_6$ ceramics sintered at 900 °C for 3 h $CaMgSi_2O_6$ crystal possesses 30 Raman

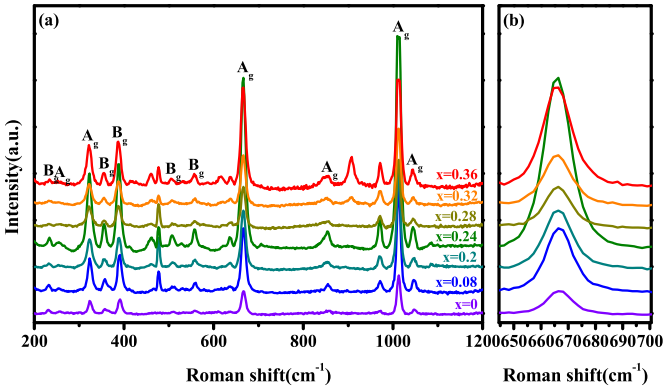

Fig. 3. Raman spectrum of the $CaMg_{0.9-x}Li_{0.2}Zn_xSi_2O_6$ (x = 0, 0.08, 0.2, 0.24, 0.28, 0.32, 0.36) ceramics sintered at 900 °C.

vibrational modes according to the space group analysis: $\Gamma_{Roman} = 14A_g + 16B_g$[22]. In general, not all Raman peaks are observed, due to the following reasons:(1) some peaks are overlapped; and (2) some peaks are too weak to be detected, as shown in Fig. 3 (a). According to the literatures [6,23], Raman peaks at approx. 1000 cm^{-1} may be caused by the stretching modes of Si and non-bridged oxygen, i.e. O–Si–O bond; Raman vibration between 500 and 700 cm^{-1} is due to Si–O–Si bending/stretching mode; The peaks below 500 cm^{-1} are related to cation vibration of M1 and M2 sites. As shown in Fig. 3 (a), Raman peak at around 905 cm^{-1}, appearing at x = 0.32, is attributed to the symmetric vibrations of Si_2O_7 dimmer in $Ca_2ZnSi_2O_7$ [17], which is in agreement with XRD analysis. The observed Raman shift reflects the short-range ordering, and the full width at half maximum (FWHM) is closely related to defects and cation disorder. A remarkable shift of Raman peaks is shown in Fig. 3 (b), indicating the short-range ordering of composites significantly change, and the shifting trend is presented in Fig. 8. In addition, FWHM of Raman peaks at 666 cm^{-1} also vary notably with the substitution content in Fig. 9. It reveals that defects and cation disorder of the samples change with increasing x value.

The grain size, pore distribution and microscopic appearance of the studied ceramics were preliminarily characterized by SEM. Fig. 4 (a)-(g) show SEM images of the $CaMg_{0.9-x}Li_{0.2}Zn_xSi_2O_6$ ceramics sintered at 900 °C for 3 h. The composites with Zn^{2+} substitution are significantly denser than those without Zn^{2+} substitution when sintered at the same temperature, demonstrating the effect of Zn^{2+} on promoting ceramic densification. In the case of grain boundaries, these are slightly miscible and blurry, which might be caused by the fact that the grains did not grow well in the multiphase system. The size distributions of the $CaMg_{0.9-x}Li_{0.2}Zn_xSi_2O_6$ ($0 \le x \le 0.28$) ceramics sintered at 900 °C for 3 h are displayed in Fig. 5, which show that when $0.08 \le x \le 0.28$ the grain size remains approx. constant (the average grain size is around 0.5 μm). However, when $x \ge 0.32$, the grains begin to grow abnormally and their size is gradually evenly distributed. The second phases are clearly distinguishable, as shown in Fig. 4 (f) and 4 (g). Furthermore, the grains' morphology also changes, which influences microwave dielectric properties.

The bulk density of the $CaMg_{0.9-x}Li_{0.2}Zn_xSi_2O_6$ ceramics sintered at different temperatures and relative density, ρ_r of the samples sintered at 900 °C are described in Fig. 6 (a) and 6 (b), respectively. ρ_r was calculated using Eq. (3), in which ρ_{theo} was obtained through Eq. (2) based on the mixture rules [24]. Without substitution, the bulk density of the composites increases with sintering temperature, and appropriate substitution of Zn^{2+} improves the density under the same temperature. The bulk density of the samples sintered at 900 °C agreed well with ρ_r, and coincides with the microstructure that displays the densest specimen is x = 0.32. The relative density ranges from 93.64% to 96.29% with substitution, demonstrating that great densification can be achieved when sintered at 900 °C.

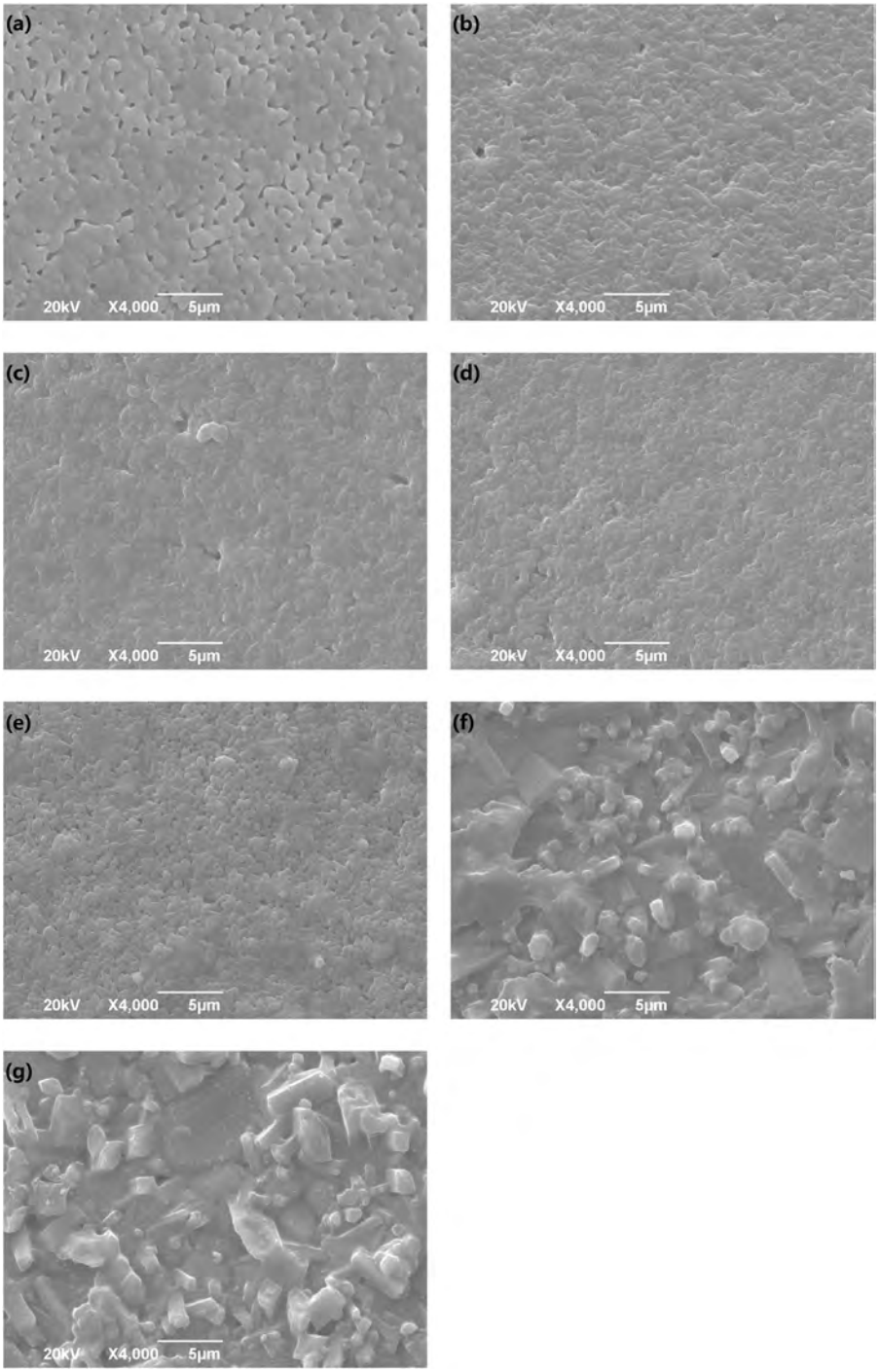

Fig. 4. SEM images of the $CaMg_{0.9-x}Li_{0.2}Zn_xSi_2O_6$ (x = 0, 0.08, 0.2, 0.24, 0.28, 0.32, 0.36) ceramics sintered at 900 °C.

The microwave dielectric properties of permittivity ε_r and dielectric loss are closely related to the second phases in multi-phase ceramics. The theoretical values of ε_r and $Q \times f$ can be calculated according to the mixing rules [25] using Eqs. (5) and (6):

$$\ln \varepsilon_r = V_1 \ln \varepsilon_{r_1} + V_2 \ln \varepsilon_{r_2} \tag{5}$$

$$\frac{1}{Q \times f} = \frac{V_1}{(Q \times f)_1} + \frac{V_2}{(Q \times f)_2} \tag{6}$$

where V_1 and V_2 represent the volume fraction while [ε_{r1}, $(Q \times f)_1$] and [$(Q \times f)_2$, ε_{r2}] correspond to the microwave dielectric properties of phase 1 and phase 2, respectively. ε_r and $Q \times f$ value of phases: $CaSiO_3$ [26], Li_2SiO_3 [27], Li_2ZnSiO_4 [28] and $Ca_2ZnSi_2O_7$ [18], produced in the samples are listed in Table 2. The calculated dielectric constant, $\varepsilon_{r\text{-}cal}$ is shown in Fig. 8. Experimental ε_r and $Q \times f$ value of the $CaMg_{0.9-x}Li_{0.2}Zn_xSi_2O_6$ ceramics sintered at different temperatures are presented in Fig. 7 (a) and 7 (b), respectively.

Fig. 7 (a) shows permittivity change trend of the $CaMg_{0.9-x}Li_{0.2}Zn_xSi_2O_6$ samples sintered at 900 °C, 925 °C and 950 °C is the same. ε_r presents an increase with increasing x value, except for a slight decrease observed at x = 0.28, whereas those sintered at 875 °C display a peak at x = 0.2. This contrasting result was mainly due to that the ceramics were not sufficiently sintered at 875 °C. Generally, ε_r is extremely sensitive toward density, second phase and ionic polarizability. Theoretical ionic polarizability, α_{theo} was calculated using Eq. (7) based

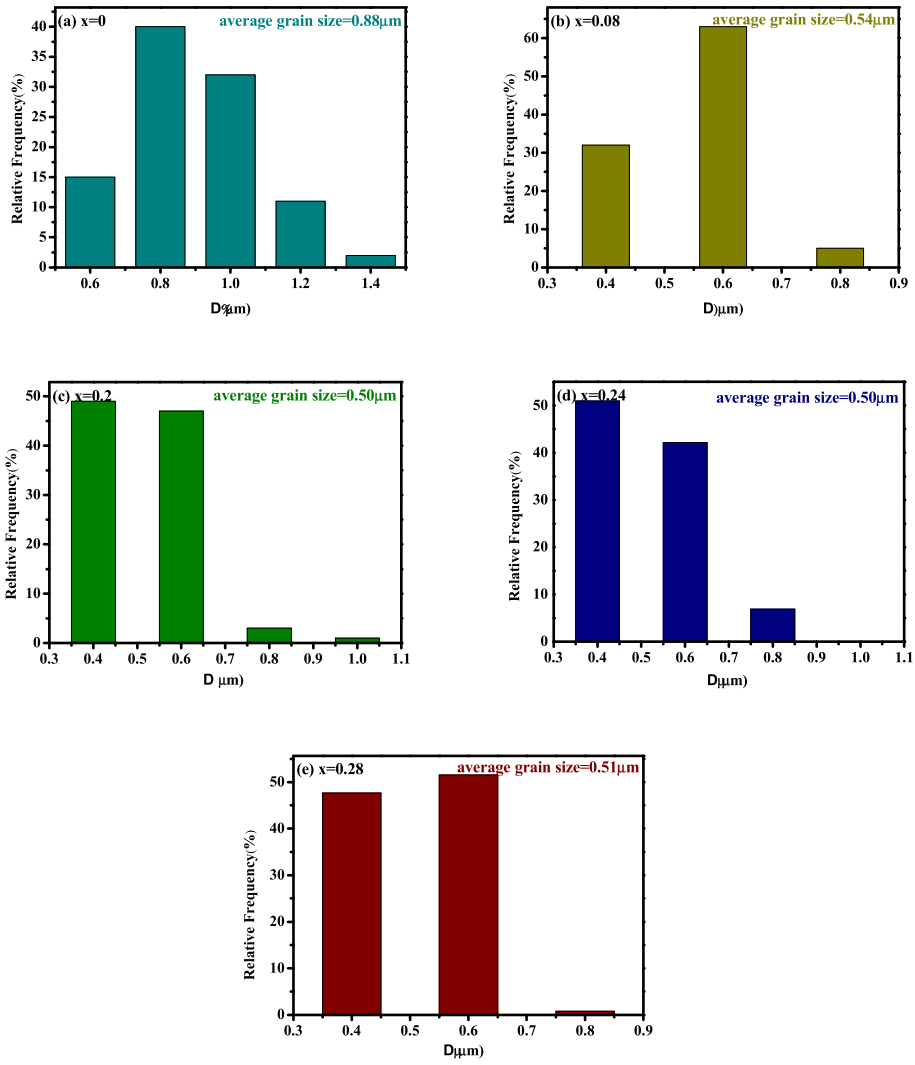

Fig. 5. The grain size distribution of the $CaMg_{0.9-x}Li_{0.2}Zn_xSi_2O_6$ (x = 0, 0.08, 0.2, 0.24, 0.28) ceramics sintered at 900 °C.

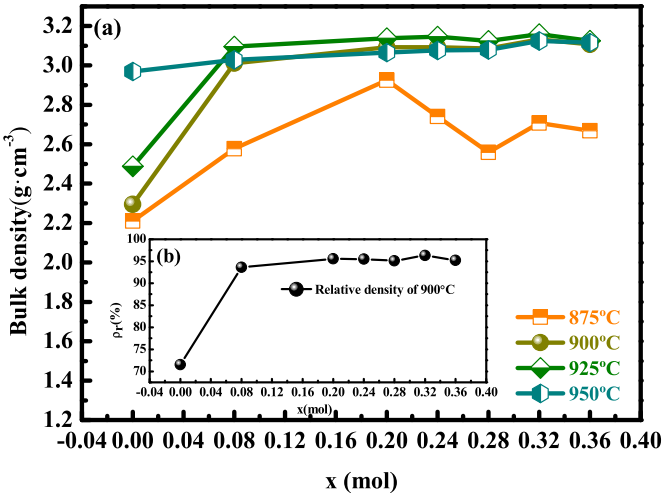

Fig. 6. (a) The bulk density of the $CaMg_{0.9-x}Li_{0.2}Zn_xSi_2O_6$ (x = 0, 0.08, 0.2, 0.24, 0.28, 0.32, 0.36) ceramics sintered at different temperatures; (b) The relative density (ρ_r) of the ceramic samples sintered at 900 °C.

on the additive rule [29], as presented in Fig. 8. In addition, Fu et al. [21] found that dielectric constant correlated inversely with Raman shift of vibration modes, and the Raman peaks shifted to higher

Table 2
Microwave dielectric properties and sintering temperature of the compounds in $CaMg_{0.9-x}Li_{0.2}Zn_xSi_2O_6$ ceramics.

	ε_r	Q × f (GHz)	τ_f (ppm/°C)	Sintering temperature (°C)	Ref.
$CaSiO_3$	6.69	25,398	−60	1000	[26]
Li_2SiO_3	7.7	9849	–	1050	[27]
Li_2ZnSiO_4	5.8	14,700	−96.6	1250	[28]
$Ca_2ZnSi_2O_7$	10.2	14,000	−30	1325	[18]

frequency indicated the decrease of polarizability. As shown in Fig. 8, Raman shift has an almost continuous decline, which is exactly opposite to the dielectric constant, implying that the polarizability increases with Zn^{2+} substitution for Mg^{2+} because of greater polarizability of Zn^{2+}(2.03 Å^3) compared to that of Mg^{2+}(1.34 Å^3). However, ε_r does not show a linear change with x value but α_{theo} does. Instead, it is in the same trend with that of the bulk density and relative density in Fig. 6, when x ≤ 0.32. Composites with a higher density obtain a bigger dielectric constant. However, ε_r changes from 7.51 to 7.53 when x alters from 0.28 to 0.32, which is also attributed to that $Ca_2ZnSi_2O_7$ phase possesses a relatively large ε_r (10.2) [18]. As shown in Fig. 8, when x ≥ 0.32 the calculated permittivity $\varepsilon_{r\text{-cal}}$ coincides well with ε_r (the measured values).

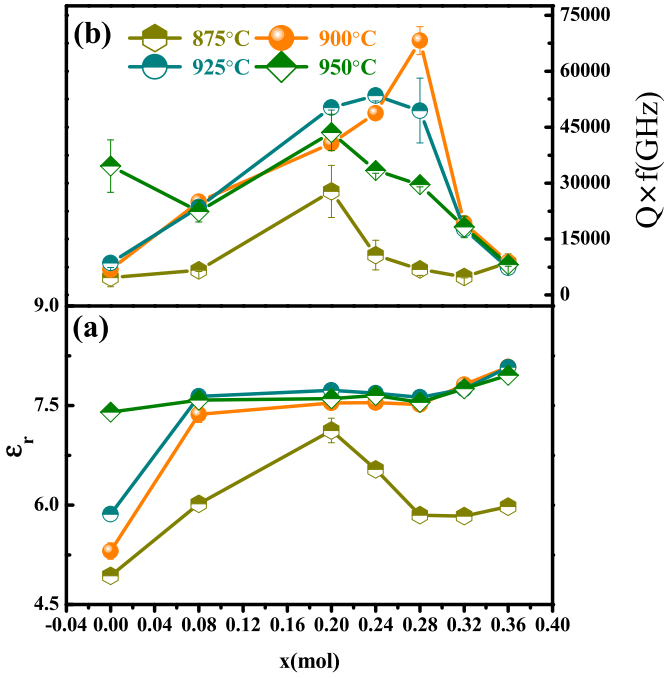

Fig. 7. (a) The quality factor ($Q \times f$) (b) and dielectric constant (ε_r) of the $CaMg_{0.9-x}Li_{0.2}Zn_xSi_2O_6$ (x = 0, 0.08, 0.2, 0.24, 0.28, 0.32, 0.36) ceramics sintered at different temperatures.

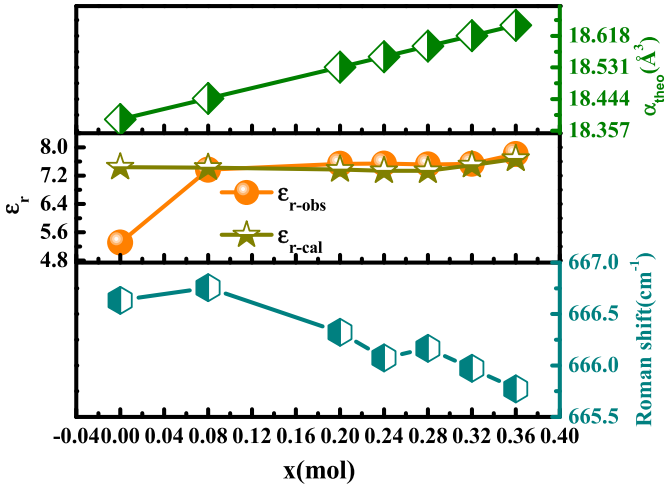

Fig. 8. Theoretical ionic polarizability (α_{theo}), dielectric constant (ε_r), dielectric constant calculated by the mixture rules ($\varepsilon_{r\text{-}cal}$) and Raman shift of peaks at 666 cm^{-1} of the $CaMg_{0.9-x}Li_{0.2}Zn_xSi_2O_6$ (x = 0, 0.08, 0.2, 0.24, 0.28, 0.32, 0.36) ceramics sintered at 900 °C.

$$\alpha_{theo}(CaMg_{0.9-x}Li_{0.2}Zn_xSi_2O_6) = \alpha_{Ca} + (0.9 - x)\alpha_{Mg} + 0.2\alpha_{Li} + x\alpha_{Zn} + 2\alpha_{Si} + 6\alpha_O \quad (7)$$

Fig. 7 (b) shows that $Q \times f$ values of the samples sintered at different temperature firstly increase and then decline after reaching maximum value, and a smaller optimum Zn^{2+} substitution content is required for a higher sintering temperature to obtain optimal performance. Samples sintered at 900 °C attain optimal $Q \times f$ value with x = 0.28. $Q \times f$ value of microwave dielectric ceramics depends on the second phase as well as density. Compared with relative density in Fig. 6, $Q \times f$ value varies in the contrast direction. Additionally, $Q \times f$ value is unaffected by density when composites are sufficiently dense. Also, $Q \times f$ values calculated using Eq. (6) do not agree with the observed values. However, $Q \times f$ values of all second phases (Table 2) are

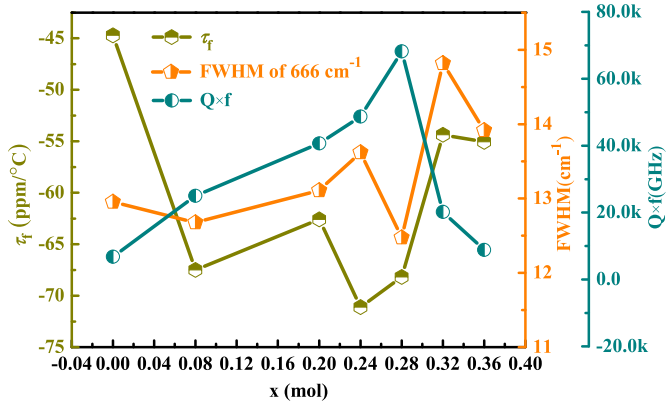

Fig. 9. τ_f, FWHM of Raman peaks at 666 cm^{-1} and quality factor ($Q \times f$) of the $CaMg_{0.9-x}Li_{0.2}Zn_xSi_2O_6$ (x = 0, 0.08, 0.2, 0.24, 0.28, 0.32, 0.36) ceramics sintered at 900 °C.

not comparable with that of $CaMgSi_2O_6$. Hence, Li_2ZnSiO_4 occurring in ceramics may possess a higher $Q \times f$ value in comparison with the reported one and $Q \times f$ values of the ceramics simultaneously change with the weight ratio of Li_2ZnSiO_4. Moreover, FWHM of Raman peak at 666 cm^{-1} shows the same trend in $Q \times f$ value with the ion substitution except at x = 0.28. Therefore, composites with such Zn^{2+} content might have lower cation disorder and might be one reason led to the highest $Q \times f$ value [30].

τ_f correlates well with the structure of ceramics and is influenced by the second phase. τ_f values of the $CaMg_{0.9-x}Li_{0.2}Zn_xSi_2O_6$ ceramics sintered at 900 °C are presented in Fig. 9. The curve varies nonlinearly with x value, which conforms to the logarithmic rule: $\tau_f = \sum V_i \tau_{fi}$, where V_i and τ_{fi} represent the volume fraction and temperature coefficient of resonant frequency of phase i, respectively. However, τ_f exhibits a similar changing trend with that of Raman FWHM at 666 cm^{-1} (Fig. 9). High FWHM value means high degree of cation disorder that may cause a negative movement of τ_f value, so cation disorder is not the dominant factor influencing τ_f but the second phase is [17,22]. Furthermore, τ_f values of the ceramics were not suitable and required further adjustment for LTCC application. Ion substitution was a attemptable method and Lai et al. [7] have reported that moderate substitutions of Cu^{2+} ions for Mg^{2+} ions could adjust τ_f by regulating MgO_6 octahedral distortion. Therefore, in next work we will adjust τ_f value through further ion substitution and carry out co-firing experiments of the ceramic material ($\tau_f \sim 0$) with Ag to evaluate the chemical compatibility and make the material more suitable for LTCC application.

4. Conclusions

In this study, microwave dielectric properties of the $CaMg_{0.9-x}Li_{0.2}Zn_xSi_2O_6$ ceramics, of which low temperature sintering was realized without any sintering aid, were investigated on the basis of phase composition, structure and density. $CaMgSi_2O_6$ was identified as the major phase and multiple second phases were indexed by XRD. The results of Rietveld refinement on XRD data indicated that Zn^{2+} substituting for Mg^{2+} had great impact on the structural characteristics and phase constitutes of the ceramics. Zn^{2+} also affected the densification of the ceramics, as identified by SEM photos. Raman shift was closely related to ε_r. The comprehensive action of the abovementioned factors influenced the performance of the $CaMg_{0.9-x}Li_{0.2}Zn_xSi_2O_6$ ceramics, and excellent microwave dielectric properties of: $Q \times f$ = 68,190 GHz, ε_r = 7.51, and τ_f = −68 ppm/°C were obtained for the sample with x = 0.28 and sintered at 900 °C.

Declaration of competing interest

The authors declare that they have no known competing financial interests or personal relationships that could have appeared to influence the work reported in this paper.

Acknowledgements

This work was supported by the National Natural Science Foundation of China under Grant Nos. U1809215, 61871069 and 61771104.

References

[1] Y.H. Zhang, J.J. Sun, N. Dai, Z.C. Wu, H.T. Wu, C.H. Yang, Crystal structure, infrared spectra and microwave dielectric properties of novel extra low-temperature fired $Eu_2Zr_3(MoO_4)_9$ ceramics, J. Eur. Ceram. Soc. 39 (2019) 1127–1131.
[2] Y. Zhang, H. Wu, Crystal structure, infrared spectra and microwave dielectric properties of novel extra low-temperature fired $Eu_2Zr_3(MoO_4)_9$ ceramics, J. Am. Ceram. Soc. 102 (2019) 4092–4102.
[3] H.W. Chen, H. Su, H.W. Zhang, T.C. Zhou, B.W. Zhang, J.F. Zhang, X.l. Tang, Low-temperature sintering and microwave dielectric properties of $(Zn_{1-x}Co_x)_2SiO_4$ ceramics, Ceram. Int. 40 (2014) 14655–14659.
[4] R. Peng, H. Su, D. An, Y. Lu, Z. Tao, D. Chen, L. Shi, Y. Li, The sintering and dielectric properties modification of Li_2MgSiO_4 ceramic with Ni^{2+}-ion doping based on calculation and experiment, J. Mater. Res. Technol. 9 (2020) 1344–1356.
[5] X.Q. Song, K. Du, J. Li, X.K. Lan, W.Z. Lu, X.H. Wang, W. Lei, Low-fired fluoride microwave dielectric ceramics with low dielectric loss, Ceram. Int. 45 (2019) 279–286.
[6] Y. Lai, H. Su, G. Wang, X. Tang, X. Huang, X. Liang, H. Zhang, Y. Li, K. Huang, X.R. Wang, Low-temperature sintering of microwave ceramics with high Qf values through LiF addition, J. Am. Ceram. Soc. 102 (2019) 1893–1903.
[7] Y. Lai, X. Tang, X. Huang, H. Zhang, X. Liang, J. Li, H. Su, Phase composition, crystal structure and microwave dielectric properties of $Mg_{2-x}Cu_xSiO4$ ceramics, J. Eur. Ceram. Soc. 38 (2018) 1508–1516.
[8] X.Q. Song, W.Z. Lu, X.C. Wang, X.H. Wang, G.F. Fan, R. Muhammad, W. Lei, Sintering behaviour and microwave dielectric properties of $BaAl_{2-2x}(ZnSi)_xSi_2O_8$ ceramics, J. Eur. Ceram. Soc. 38 (2018) 1529–1534.
[9] H.H. Guo, D. Zhou, W.F. Liu, L.X. Pang, D.W. Wang, J.Z. Su, Z.M. Qi, Microwave dielectric properties of temperature-stable zircon-type (Bi, Ce)VO_4 solid solution ceramics, J. Am. Ceram. Soc. 103 (2019) 423–431.
[10] J.J. Bian, D.W. Kim, K.S. Hong, Glass-free LTCC microwave dielectric ceramics, Mater. Res. Bull. 40 (2005) 2120–2129.
[11] T. Joseph, M.T. Sebastian, H. Sreemoolanadhan, V.K.S. Nageswari, Effect of glass addition on the microwave dielectric properties of $CaMgSi_2O_6$ ceramics, Int. J. Appl. Ceram. Technol. 7 E98-E106.
[12] M.K. Zitani, T. Ebadzadeh, S. Banijamali, R. Riahifar, C. Rüssel, S.K. Abkenar, H. Ren, High quality factor microwave dielectric diopside glass-ceramics for the low temperature co-fired ceramic (LTCC) applications, J. Non Crys. Solids 487 (2018) 65–71.
[13] H. Sun, Q. Zhang, H. Yang, J. Zou, $(Ca_{1-x}Mg_x)SiO_3$: a low-permittivity microwave dielectric ceramic system, Mater. Sci. Eng. B 138 (2007) 46–50.
[14] A. Ullah, H. Liu, H. Hao, J. Iqbal, Z. Yao, M. Cao, Q. Xu, Effect of Zn substitution on the sintering temperature and microwave dielectric properties of $MgSiO_3$-based ceramics, Ceram. Int. 43 (2017) 484–490.
[15] D. Thomas, M.T. Sebastian, Effect of Zn^{2+} substitution on the microwave dielectric properties of LiMgPO4 and the development of a new temperature stable glass free LTCC, J. Eur. Ceram. Soc. 32 (2012) 2359–2364.
[16] X. Jing, X. Tang, W. Tang, Y. Jing, Y. Li, H. Su, Effects of Zn^{2+} substitution on the sintering behaviour and dielectric properties of $Li2Mg_{1-x}Zn_xSiO_4$ ceramics, Appl. Phys. A 125 (2019).
[17] H. Li, C. Cai, Q. Xiang, B. Tang, S. Yu, J. xiao, H. Luo, S. Zhang, Raman, complex chemical bond and structural studies of novel $CaMg_{1-x}(Mn_{1/2}Zn_{1/2})_xSi_2O_6$ (x = 0-0.1) ceramics, Ceram. Int. 45 (2019) 23157–23163.
[18] J. Zhang, Y. Zhou, Z. Yue, Low-temperature sintering and microwave dielectric properties of LiF-doped $CaMg_{1-x}Zn_xSi_2O_6$ ceramics, Ceram. Int. 39 (2013) 2051–2058.
[19] M. Zhong, H. Su, X. Jing, Y. Li, Q. Lu, Y. Jing, Crystal structure and microwave dielectric properties of $Li_2Mg_{0.6-x}Co_xZn_{0.4}SiO_4$ ceramic for LTCC applications, Ceram. Int. 46 (2020) 13095–13101.
[20] H. Wang, D. Li, Q. Yang, R. Lei, H. Ma, S. Xu, Sintering behavior and microwave dielectric properties of $CaMgSi_2O_6$ ceramics with Al_2O_3 addition, Mater. Res. Bull. 54 (2014) 66–72.
[21] Z. Fu, C. Li, J. Ma, Y. Wu, Low temperature sintering mechanism for $Li_2Mg_3SnO_6$ microwave dielectric ceramics, Mater. Sci. Eng. B 250 (2019).
[22] B. Tang, Q. Xiang, Z. Fang, X. Zhang, Z. Xiong, H. Li, C. Yuan, S. Zhang, Influence of Cr^{3+} substitution for Mg^{2+} on the crystal structure and microwave dielectric properties of $CaMg_{1-x}Cr_{2x/3}Si_2O_6$ ceramics, Ceram. Int. 45 (2019) 11484–11490.
[23] Y. Lai, H. Su, G. Wang, X. Tang, X. Liang, X. Huang, Y. Li, H. Zhang, C. Ye, X.R. Wang, Improved microwave dielectric properties of $CaMgSi_2O_6$ ceramics through CuO doping, J. Alloys Compd. 772 (2019) 40–48.
[24] T. Qin, C. Zhong, Y. Qin, B. Tang, S. Zhang, Low-temperature sintering mechanism and microwave dielectric properties of $ZnAl_2O_4$-LMZBS composites, J. Alloys Compd. 797 (2019) 744–753.
[25] J. Zhang, R. Zuo, J. Song, Y. Xu, M. Shi, Low-loss and low-temperature firable $Li_2Mg_3SnO_6$-Ba_3 $(VO_4)_2$ microwave dielectric ceramics for LTCC applications, Ceram. Int. 44 (2018) 2606–2610.
[26] L. Ouyang, W. Wang, H. Fan, Z. Weng, W. Wang, H. Xue, Sintering behavior and microwave performance of $CaSiO_3$ ceramics doped with $BaCu(B_2O_5)$ for LTCC applications, Ceram. Int. 45 (2019) 18937–18942.
[27] Y. Lai, X. Tang, H. Zhang, X. Huang, J. Li, H. Su, Relationship between the structure and microwave dielectric properties of non-stoichiometric $Li_{2+x}SiO3$ ceramics, Ceram. Int. 43 (2017) 2664–2669.
[28] G. Dou, D. Zhou, S. Gong, M. Guo, Low temperature sintering and microwave dielectric properties of Li_2ZnSiO_4 ceramics with ZB glass, J. Mater. Sci. Mater. Electron. 24 (2012) 1601–1607.
[29] V. Dimitrov, S. Sakka, Electronic oxide polarizability and optical basicity of simple oxides. I, J. Appl. Phys. 79 (1996) 1736–1740.
[30] H. Li, X. Chen, Q. Xiang, B. Tang, J. Lu, Y. Zou, S. Zhang, Structure, bond characteristics and Raman spectra of $CaMg_{1-x}Mn_xSi_2O_6$ microwave dielectric ceramics, Ceram. Int. 45 (2019) 14160–14166.